



The long-term optical activity of the propellers AE Aquarii and AR Scorpii

Vojtěch ŠIMON1,2,*

- ¹Astronomical Institute of the Czech Academy of Sciences, 25165 Ondřejov, Czech Republic
- ²Czech Technical University in Prague, Faculty of Electrical Engineering, 16627 Prague, Czech Republic

Received 2019 October 31; Accepted 2020 January 31

Abstract

This analysis of the long-term optical activity of the propellers AE Aqr and AR Sco uses data from the Catalina Real-time Transient Survey, DASCH, and AAVSO. The site and character of the emissions from the phenomena caused by the magnetic field of the white dwarf (WD) vary from system to system. The histogram of intensities of the ensemble of flares of AE Aqr suggests that the long-term activity consists of a large variety of the peak magnitudes of the flares, with the probability of their detection gradually decreasing with increasing intensity. Any increase of activity only leads to an increase of the number of blobs of the transferring matter. We also detected a season with a transient decrease or even a cessation of the mass outflow from the donor to the lobe of the WD. The very strong orbital modulation of AR Sco is most stable in the phases of the extrema of brightness for about a century; its minor changes suggest that the trailing side of the synchrotron-emitting region is more unstable than the leading side.

Key words: accretion, accretion disks — magnetic fields — novae, cataclysmic variables — radiation mechanisms: general — white dwarfs

1 Introduction

Cataclysmic variables (CVs) are binaries with an orbital period $P_{\rm orb}$ whose length is typically several hours. Matter transfers onto the white dwarf (WD) from its lobe-filling companion. See Warner (1995) for a review.

Magnetic braking (angular momentum loss in a stellar wind that is magnetically coupled to the secondary star) plays a big role in the evolution of CVs (Rappaport et al. 1983). This braking is sharply reduced when the massdonating star undergoes large changes of its internal structure; this explains the 2–3 hr "gap" in the distribution of orbital periods, $P_{\rm orb}$, of CVs. This was also confirmed by the new method of Gänsicke et al. (2009).

If CVs exhibit long-term mass-transfer-rate fluctuations, the expected variability timescales are so long that other tracers of the mass-transfer rate (e.g., WD temperatures) become unreliable (Knigge et al. 2011). The tidal and rotational deformation of the Roche-lobe-filling stars produces about 4.5% radius inflation below the period gap and about 7.9% above; donor bloating due to irradiation is probably at most comparable to these effects.

The current type of CV is determined by its previous evolution (Podsiadlowski et al. 2003). Their simulations show that CVs with $P_{\rm orb} > 5$ hr are dominated by evolved, relatively massive, systems. These systems are the progenitors of ultracompact systems. The large variety of behaviors exhibited by CVs is due to the nuclear evolution of the donor and high-mass donors according to Goliasch and Nelson (2015). They show that the ranges of $P_{\rm orb}$, the mass-transfer rates, and the properties of the donor in CVs cover a very wide range of values. They also reveal a population of evolved systems that have remarkably lower

^{*}E-mail: simon@asu.cas.cz

mass-transfer rates. The evolved systems might thus account for the observed fraction of dwarf novae.

A model of the range of CV tracks with different evolutionary states of the donor star (Kalomeni et al. 2016) predicts CV-like systems with periods of 2–40 d and donor masses of 0.3–0.8 M_{\odot} (currently, the longest $P_{\rm orb}=5.786$ d is observed in V1017 Sgr; Salazar et al. 2017). This model also evaluated that supersoft X-ray sources are likely to be found with $P_{\rm orb}$ of 4–50 hr. The densely populated region with $P_{\rm orb}$ of 1–2 hr and low-mass donors may contain many post-period minimum CVs with very small mass-transfer rate.

The distribution of $P_{\rm orb}$ of CVs still shows some discrepancies. A significant accumulation of low-luminosity systems in the orbital period range 80–86 min is observed (Gänsicke et al. 2009). This spike is almost entirely due to the large number of CVs with very low accretion activity. Their optical spectra are dominated by emission from the WD photosphere.

Warner (1995) presented an extensive review, especially of the individual types of CVs (both with magnetized WDs and with non-magnetized WDs) and their activity. This activity is determined mainly by the mass-transfer rate from the donor to the WD, and the strength of the magnetic field of the WD. If the mass-transfer rate from the donor to the WD is between some limits, the accretion disk (if present) is subject to a thermal-viscous instability. This gives rise to the dwarf nova outbursts. A newer version of this model was presented by Hameury et al. (1998).

The strong magnetic fields of the WDs in some CVs (polars) strongly influence the mass flow (Cropper 1990) and cause strong polarization of their optical emission (Tapia 1977; Krzeminski & Serkowski 1977). The matter flows directly toward the magnetic poles of the WD synchronously spinning with $P_{\rm orb}$. No accretion disk can be formed (Cropper 1990).

In CVs with mildly magnetized WDs (B up to several megagauss), the so-called intermediate polars (IPs; Warner 1995), the accretion disk is often present, but its inner region is truncated by the magnetic field of the WD. The accretion flow of an IP is controlled by the magnetic field of the WD inside the magnetosphere (Alfvén radius) of this accretor. The spin periods of their WD are shorter than their $P_{\rm orb}$ (e.g., Patterson & Price 1981). Some intermediate polars are diskless: much of the accretion flow in V2400 Oph is not in a coherent stream, but is circling the WD, possibly as a ring of blobs (Hellier & Beardmore 2002).

The observations of magnetic CVs of Schmidt, Stockman, and Grandi (1986) were interpreted as an accretion profile which is not perfectly collimated, where the optical/IR continuum can be dominated by a low-density halo around the compact hard X-ray shock.

Norton et al. (2007, 2008) used a magnetic accretion model to investigate the accretion flows of magnetic cataclysmic variables (mCVs) throughout a range of the parameter space. They demonstrated that four types of flow are possible: disks, streams, rings, and propellers. Two possibilities for IPs with very small ratios $P_{\rm spin}/P_{\rm orb} \leq 0.01$ ($P_{\rm spin}$ referring to the spin period of the WD) exist: (a) disklike accretors, (b) strong magnetic propellers (if they are out of equilibrium).

The boundary between stable and unstable regimes of accretion onto a magnetized accretor depends almost entirely on the ratio between the magnetospheric radius and the co-rotation radius of the accretor (Blinova et al. 2016). They determined the limits of unstable, stable, and propeller regimes of accretion.

The differences between the accretor and the propeller regimes were shown by Bisikalo and Zhilkin (2012). The flow structure in mCVs is strongly influenced by asynchronous rotation of the accretor. If the rotation is rapid ($P_{\rm spin} < 0.033\,P_{\rm orb}$, "propeller"), a magnetosphere cavity is formed near the accretor and the accretion rate onto the WD dramatically falls. This also influences the long-term activity because the subsequent growth of the mass of the disk leads to matter breaking through the magnetosphere and a sharp jump in the accretion rate.

In this paper we investigate the optical long-term activity of two propellers, AE Aqr and AR Sco. Preliminary versions of part of this analysis were presented by Šimon (2013, 2014, 2018) and V. Šimon (2019).¹

2 Observations

Charge-coupled device (CCD) *V*-band observations from the ASAS-3 project² (Pojmanski 1997) of AE Aqr were obtained with a 200/2.8 camera (field of view $8^{\circ}.5 \times 8^{\circ}.5$, exposure time of 180 s, one CCD image of the field obtained per night). The Southern sky was densely observed in 2001–2009. Only observations with an assigned quality of A or B in the ASAS-3 file (column 2 in the original data file) were included in our analysis. The error bars come from column 7 in the original data file. The error bars of the observations of AE Aqr which we used varied between 0.034 and 0.064 mag, with a typical value of 0.041 mag.

V-band CCD data (sometimes supplemented by CV-band observations) of AE Aqr were also obtained from the AAVSO (American Association of Variable Star Observers)

¹ Šimon, V. 2019. Presentation at Large Surveys with Small Telescopes, 2019 March 11–13, Bamberg, Germany (doi:10789/plate/lswst/009).

^{2 (}http://www.astrouw.edu.pl/asas); (http://www.astrouw.edu.pl/asas/?page=atlas).

International database (USA).³ An inspection of the data showed that the error bars were about 0.02–0.03 mag.

The Catalina Real-time Transient Survey (CRTS; Drake et al. 2009)⁴ obtained CCD images of AR Sco in the V-band between 2005 and 2013.⁵ Usually, one CCD image or a couple of images of the field were obtained per night. The brightness uncertainties of these observations, used in the analysis, range from 0.05 mag to 0.14 mag, with a typical value of 0.065 mag.

The digitized photographic data of AR Sco were obtained from Digital Access to a Sky Century @ Harvard (DASCH; Grindlay et al. 2012; Grindlay & Griffin 2012). This database provides SExtractor-based photometry of every resolved object. The band of these data can be approximated by the *B*-band. The standard deviations of brightness of AR Sco varied from 0.06 mag to 0.45 mag, with a typical value of 0.11 mag.

3 Data analysis

An inspection of the observations showed that the uncertainty of brightness of the propellers AE Aqr and AR Sco was considerably smaller than the amplitude of the observed variations of brightness. This confirms that the observed light changes are true.

3.1 AE Agr

AE Aqr is a CV with a relatively long $P_{\rm orb}$ of 9.879744 hr (van Paradijs et al. 1989). The distance d of AE Aqr, 90.956 ± 0.462 pc, was determined from the observations with the satellite Gaia⁷ (Gaia Collaboration 2018; Bailer-Jones et al. 2018).

The optical emission of AE Aqr is often dominated by a K0–K4 donor (Echevarría et al. 2008) because of a low mass-transfer rate. The companion is a rapidly spinning magnetized WD (33.076737 s; van Paradijs et al. 1989). AE Aqr often displays flares. A typical duration of a single flare is several minutes, but these events can cluster (van Paradijs et al. 1989).

Eracleous and Horne (1996) found that the UV spectrum of flares contains the emission lines and a prominent Balmer recombination continuum. They argued that the accretion flow from the donor star is fragmented into discrete blobs that interact with the propeller that is the magnetosphere of the rapidly spinning WD. They ruled out these flares as coronal activity on the companion star or a magnetospheric

gating instability at the WD. They proposed that the flares represent the excitation of gaseous blobs upon encounter with the propeller, and their subsequent radiative cooling as they are expelled from the system.

In the interpretation of Wynn, King, and Horne (1997), most of the transferring matter in AE Aqr is ejected by the rapidly spinning magnetized WD. The system has no disk, but expels most of the transferred matter with little or no accretion. The discrepancy between the large spin-down power of the WD and the observed luminosity of AE Aqr was explained by the kinetic energy carried away by the ejecta. Blinova et al. (2019) suggested that some type of an accretion disk could form around the WD and interact with its magnetosphere. The disk–magnetosphere interaction was a strongly non-stationary process. Most of the inner disk matter was ejected into conically shaped winds, and a much smaller part accreted onto the WD.

The long-term activity of AE Aqr in the optical band is displayed in figure 1. The large scatter of the light curve in figure 1a can be explained by the activity consisting of a set of flares non-uniformly distributed in time. A typical flare (or a cluster of flares) lasts for at most several tens of minutes (van Paradijs et al. 1989). ASAS obtained one CCD image of the field per night. Although each point in figure 1a represents at most one flare in any of its phase, these observations cover a long time interval (years).

The data of AE Aqr folded with $P_{\rm orb}$ according to the ephemeris of Echevarría et al. (2008) display a large scatter caused by the real brightness variations, not by noise; the flares occur in any orbital phase (figure 1b; see also van Paradijs et al. 1989). The double-wave profile of the lower envelope of the folded light curve (remaining all the time, even when the flares are missing) is caused by the tidal deformation of the donor (van Paradijs et al. 1989). Although the number of flares varies for the individual years, the lower envelope of the light curve is not greatly influenced by the presence of these events. When the flares are missing, the profiles of the upper and lower envelopes can be considered the same.

In the interpretation, the same orbital modulation of the low state as in the active state (in which the flares occur) disfavors any significant role of the large variations of the active regions on the donor in the continuum light, although changes of the fractional spot coverage were detected in the spectral lines with Roche tomography (Hill et al. 2014, 2016). Even if formation of an accretion disk is possible in AE Aqr (Blinova et al. 2019), our data show that its contribution to the continuum *V*-band luminosity is negligible, at least in this low state. The stable modulation thus disfavors the cause of the low state by a transient change of the mode of the mass transfer (from blobs to disk).

³ Kafka, S. 2018, Observations from the AAVSO International Database (https://www.aavso.org/data-download).

^{4 (}http://crts.caltech.edu/).

^{5 (}http://nesssi.cacr.caltech.edu/cgi-bin/getcssconedbid_release2.cgi#simtable).

^{6 (}http://dasch.rc.fas.harvard.edu/lightcurve.php).

^{7 (}http://gea.esac.esa.int/archive/).

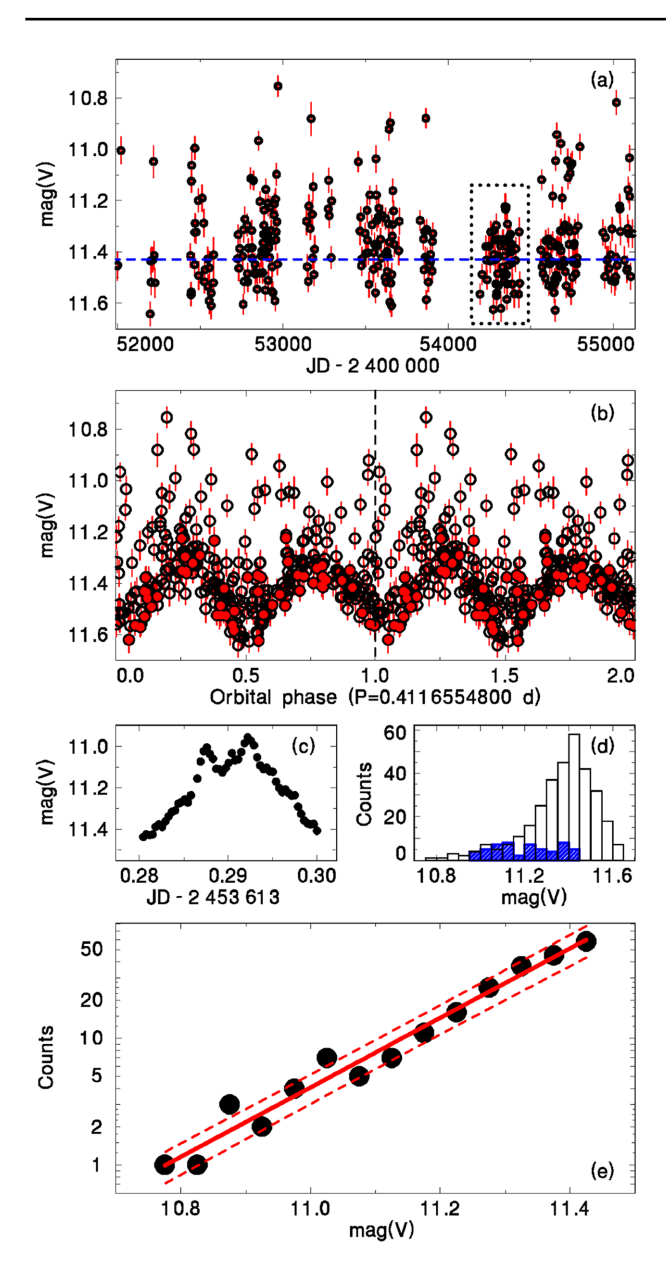


Fig. 1. (a) Long-term activity of AE Aqr in the optical band (the ASAS data, one CCD image per night). The segment with the absent flares is marked by the box. (b) The light curve folded with $P_{\rm orb}$ according to the ephemeris of Echevarría et al. (2008). The open circles represent all the data points from panel (a), while the closed circles denote the data from the box in panel (a). (c) Light curve of a flare in the *V*-band (AAVSO). (d) Histogram of the light curve of the flare from (c) (shaded) and the whole ASAS data set (empty bars). (e) Histogram of brightness of the flares from (a). Only observations of brightness higher than 11.4 mag (V) in which only the flares, not the donor's tidal variations in between the flares, dominate are considered. The standard deviation of the fit is marked. See subsection 3.1 for details. (Color online)

A season with almost absent or faint flares (the box in figure 1a) can be explained by a transient decrease or even a cessation of the mass outflow from the donor to the lobe of the WD. Such an evolution suggests a variable amount of blobs on the timescale of months. Because the flares are relatively uniformly distributed over all orbital phases

(figure 1b), the absence of flares inside the box in figure 1a disfavors an explanation by the observations being accidentally restricted to the orbital phases in which the flares are not detectable. The time season without any observed flares can be analogous to the low states in some novalikes in which the mass transfer is temporarily lowered or ceased (e.g., MV Lyr; Rosino et al. 1993). These changes suggest the time variations of activity of the donor also in AE Aqr.

In figure 1d, a histogram of brightness of an example of the light curve of a flare (or a double flare) of AE Aqr (figure 1c) is compared with the histogram of the whole data set from figure 1a. Both histograms are mutually largely divergent. While the histogram of brightness of a single flare is flat, the histogram of an ensemble of flares shows a gradual increase of the number of counts with a decreasing brightness between 11.0 and 11.5 mag (*V*).

Figure 1e shows a histogram of brightness in the ASAS observations in which AE Aqr is brighter than 11.4 mag (V). This limit assures that only the flares, not the donor's tidal variations in between the flares, are included. The histogram is log-log in the intensity scale. Although a flare in the ASAS data is represented by a single point, which might be obtained in any phase of this event, the histogram of the whole ensemble suggests that the long-term activity of AE Agr consists of a large variety of peak magnitudes and/or profiles of the flares. The probability of their detection decreases with their increasing brightness. In this context, any sign of the accretion disk which may be present in AE Agr (Blinova et al. 2019) should produce a bump superposed in figure 1e. This suggests that the continuum luminosity of this disk (if present) is overshone by the flares.

The differences between the histograms for the ensemble of the ASAS data and a single AAVSO flare in figure 1d gradually increase with a decrease of brightness for magnitudes <11.4. The standard deviation of the fit, σ_f , in figure 1d shows that the dependence of the counts on mag(V) is well defined. Although the values of the counts are mutually similar (well within the value of σ_f) for both histograms in figure 1d for magnitudes brighter than 11.15, this difference gradually increases with decreasing brightness. It is already about $3.7\,\sigma_f$ for the brightness 11.40 mag. This suggests that the peak brightnesses of the flares are not the same for all of these events. The higher the peak brightness of the flare, the less probable its occurrence.

Although the flares are relatively uniformly distributed over all orbital phases in figure 1b (the years 2001–2009), Zamanov and Latev (2017) observed most flares between the orbital phases 0.55 and 1.05 (especially 0.55–0.75) between the years 1993 and 1999. In contrast, Bruch and Grutter (1997) showed that more flares occurred during the

first half of the orbital phases between the years 1978 and 1995.

In the interpretation, anisotropy of radiation of the flare can also be involved. The optical emission radiated from the leading side of a blob when it interacts with the magnetosphere of the WD is detected mainly in the orbital phase when the observer is looking toward the leading side of this blob. A change of the position of this interaction region in the orbital phase could explain the observed dependence of the flares on this phase. A model of such processes is desirable.

The variations of the observed flares with the orbital phase can be caused by changes of the conditions which influence the motion of the streaming matter. In this context, we notice that the structures of the matter from the donor which are stable in the orbital phase and located beyond its lobe (probably kept by the magnetic field) were observed in the polar AM Her by Kafka et al. (2008, 2010). They argued that the motion of gas between the two stars is complex along magnetic field lines associated with both stars. A similar process can also be responsible for a modification of the stream in AE Agr.

Yu et al. (2019) showed that AE Aqr is similar to KIC 5608384 in the sense that both systems contain donors with signatures of having undergone significant nuclear evolution. This has led to their current very low mass-transfer rates. According to Yu et al. (2019), the secular mean accretion rate of KIC 5608384 is $\dot{m} \leq 3 \times 10^{-10} \, M_{\odot} \, \mathrm{yr}^{-1}$. According to Eracleous and Horne (1996), a rough estimate of \dot{m} is of the order of $10^{-9} \, M_{\odot} \, \mathrm{yr}^{-1}$ for AE Aqr, but more than 99% of this mass is expelled from the system by the propeller. Because of these low rates, the different strengths of the magnetic fields of their WDs manifest themselves by the flares in the propeller AE Aqr and by the very infrequent dwarf nova outbursts in the non-magnetic KIC 5608384.

The flares of AE Aqr, thought to arise from collisions between the regions in the material expelled from the CV after an interaction with the rotating magnetosphere of the WD (Wynn et al. 1997), obey a similar histogram of brightness (figure 1e) to the infrared (K_s -band) flares (Genzel et al. 2003; Witzel et al. 2012) from Sgr A*, the supermassive central black hole of our Galaxy. Meyer et al. (2006) linked the flares of Sgr A* to the synchrotron emission from the hot spots in the accretion disk near the last stable orbit of the black hole. A comparison of activities of AE Agr and Sgr A* shows that similar profiles of the histogram of intensities of the flares exist for the dramatically different optical luminosities of the flares, emission mechanisms, and masses and types of the central compact objects. According to Genzel et al. (2003), the infrared flares in Sgr A* suggest turbulence, magnetic reconnection, or shocks. The flare is then due to

an acceleration event, similar to a solar flare, rather than an enhanced accretion. Analogously, tearing of the inflowing matter in the magnetosphere of a rapidly spinning WD may cause the flares in AE Aqr.

3.2 AR Sco

AR Sco contains an M5V component and a very rapidly spinning WD (1.97 min; Marsh et al. 2016). The pulsed luminosity is powered by the spin-down of this highly magnetized WD, while the mass transfer is much less important (Buckley et al. 2017). The optical activity is dominated by a very strong orbital modulation (Littlefield et al. 2017) of the system with $P_{\rm orb}$ of 3.56 hr (Marsh et al. 2016). The WD is a nearly perpendicular rotator, its open field line beams sweep the late-type companion's stellar wind. Synchrotron radiation of the shocked electrons of the wind can explain the spectral energy distribution of AR Sco and its strong orbital modulation (Geng et al. 2016).

Figure 2 shows the long-term light curve of AR Sco (only the detections with AR Sco at least 0.25 mag brighter than the plate limit). A linear fit to the data with the orbital phases 0.3–0.6 (around a flat peak; see figure 2b) shows a stable peak brightness on the timescale of decades.

Figure 2b shows the data folded with $P_{\rm orb}$ according to the ephemeris of Marsh et al. (2016). Phase 0.0 corresponds to the inferior conjunction of the late-type star.

The profile of the modulation of the DASCH data was smoothed by the HEC13 code,8 written by P. Harmanec. This code is based on the method of Vondrák (1969), who improved the original method of Whittaker and Robinson (1946). The method is based on minimizing the value $P = F + \lambda^2 S$, where $F = \sum p(y_i - y_i')^2$ denotes the degree of smoothing (p being the weight, y being the smoothed data, and y' the observed value of the variable), $S = \sum (\Delta^3 y_i)^2$ is the sum of the squares of the third differences of the smoothed curve called the measure of roughness of the curve, and λ^2 is a constant to be selected and defines how much the curve will be smoothed. A full description of the method can be found in Vondrák (1969). This method can fit a smooth curve to the non-equidistant data no matter what their profile is. HEC13 makes use of two input parameters, ϵ (in dimensionless units) and ΔT . The quantity $\epsilon = 1/\lambda^2$ determines how "tight" the fit will be, that is, if only the main profile or also the high-frequency variations are to be reproduced. The quantity ΔT is the time interval over which the data are binned before smoothing. The resulting fit consists of the mean points, calculated to the individual observed points of the curve.

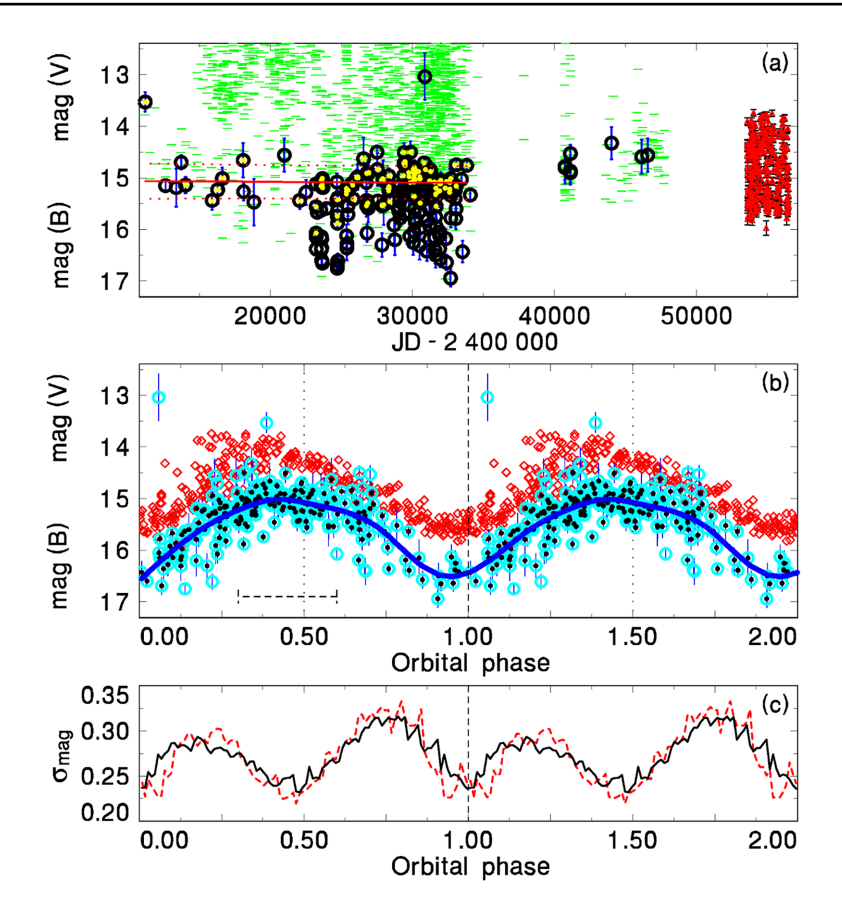


Fig. 2. (a) Long-term light curve of AR Sco from DASCH data (open circles) and CRTS data (open triangles). The data between phases 0.3–0.6 prior to JD 2 434 076 (a gap in the data) are marked by the closed circles. A linear fit to them with its standard deviation is included. (b) Observations folded with $P_{\rm orb}$ according to the ephemeris of Marsh et al. (2016). The horizontal line marks phases 0.3–0.6. The open diamonds represent the CRTS data. The open circles mark the DASCH data. The smooth line denotes the 5% trimmed HEC13 fit to the DASCH data (closed circles). (c) The moving averages of the standard deviations of the residuals of the 5% trimmed HEC13 fit for Q = 0.1 (the dashed line) and Q = 0.15 phase (the solid line). See subsection 3.2 for details. (Color online)

A set of the HEC13 fits to the folded data with different ϵ and ΔT was generated and submitted for inspection. The resulting fit with $\epsilon = 10^7$, $\Delta T = 0.05$ yields a good result. The influence of the most distant points (e.g., flares) can be lowered if the most deviating residuals of the fit are removed (the 5% most negative and 5% most positive residuals in our case). This data set was fitted again by the HEC13 code with the aforementioned input values. It can be called a 5% trimmed fit. This profile revealed that the DASCH modulation in particular contains a less steep and non-linear decaying branch (with a superimposed bump?) in comparison with the CRTS data (figure 2b).

The moving averages of the standard deviations of the residuals of the 5% trimmed HEC13 fit, σ_{mag} , were smoothed by the two-sided moving averages. This method is described in Brockwell and Davis (1987). The half-widths Q = 0.1 and Q = 0.15 phase were used (figure 2c).

We find that although the orbital modulation is unstable in some phases, the peak-to-peak amplitude does not change significantly (figure 2b). The value of σ_{mag} is most

stable in the phases of the extrema of brightness. It is true that various lengths of the exposure time of the individual plates can cause a scatter in the phases of the folded light curve in which the brightness rapidly varies. However, the value of σ_{mag} is bigger near phase 0.7 than near phase 0.2, although the rate of change of brightness is bigger near phase 0.2. This suggests that the modulation is most unstable near phase 0.7. This therefore suggests that the trailing side of the synchrotron-emitting region is more unstable than the leading side. Also, a comparison of the DASCH light curve in figure 2b with the CRTS data or the observations of Littlefield et al. (2017) suggest either that various regions of the synchrotron-emitting region are variable on the timescale of years or that the spectral energy distribution of synchrotron emission is more complicated.

The stability of the modulation also speaks against precession of the axis of the magnetic poles of the WD, at least on a timescale shorter than or comparable to about a century. This constrains the possible explanation of Katz (2017); this precession was disproved by Peterson, Little-field, and Garnavich (2019).

We also searched for a possible relation of this orbital modulation of AR Sco and the activity of the cool star. In this regard we notice that Bianchini (1990) showed that both single main-sequence stars and late-type secondary components of CVs display cycles of activity. Their cycle lengths are between ~ 3 and ~ 17 yr, peaking around 6 yr. Such cycles also influence the coronae, as suggested by the anticorrelation of the X-ray/UV variations and the optical brightness during a 7 yr cycle in Proxima Centauri (Wargelin et al. 2017). If such a cycle were also present in AR Sco, it could also influence the number of electrons for the generation of its synchrotron emission. However, the amplitude of the orbital modulation in figures 2a and 2b appears unaffected by such a possible cycle. In the context of Wargelin et al. (2017), there is also a possibility that if the coronal activity of the late-type star in AR Sco is high all the time, with the surface covered by active regions, then this star can remain in the vicinity of the peak of the cycle all the time.

The distance of 117.37 ± 0.57 pc of AR Sco (Gaia Collaboration 2018; Bailer-Jones et al. 2018) shows that the absolute magnitude $M_{\rm opt}$ varies between about 9.5 and 11.5. It therefore resides in a very long deep low state, at least for several decades. Its $M_{\rm opt}$ is similar to that in the low states of some nova-likes like MV Lyr (Rosino et al. 1993; Pavlenko 1996; Pavlenko & Shugarov 1998) and the IP 1223 Sgr (Garnavich & Szkody 1988), but this state is much longer.

Rapid spin of the WD (Marsh et al. 2016) suggests that AR Sco underwent an evolution with a high mass-transfer rate. We ascribe the current low luminosity (no mass transfer between the components) of AR Sco to the previous evolution of its donor. In this regard, a model of evolution tracks of CVs (Goliasch & Nelson 2015) revealed a very broad range of mass-transfer rates in systems shortly before entering the period gap. The model of Goliasch and Nelson (2015) also shows a population of CVs with remarkably low mass-transfer rates because they contain the evolved donors. A model of the history of AR Sco, taking into account the spinning magnetic field of the WD and its influence on the mass transfer, is desirable.

4 Conclusions

We have shown the long-term optical activity of the propellers AE Aqr and AR Sco. Although these CVs reside near the optical luminosity of the low states of nova-likes, they are still active especially on the timescale of less than a day.

The optical emission of the surfaces of the WDs is not a strong contributor in these two propellers. The site and character of the emission of the phenomena caused by the magnetic field of the WD vary from system to system. The character of the activity in these propellers also depends on the inclination of the axis of the bipolar magnetic field of the WD.

Rapid spin periods of the WDs of AE Aqr and AR Sco suggest that these systems are the results of CVs which underwent a phase of a very high mass-transfer rate (in AE Aqr $\sim 10^{-6}~M_{\odot}~\rm yr^{-1}$; Meintjes 2002; Schenker et al. 2002). These phases thus finished with a transition to a very low mass-transfer rate. They may belong to the population of evolved systems that have remarkably lower mass-transfer rates now, as revealed by the model of Goliasch and Nelson (2015).

Acknowledgment

This study was supported by EU project H2020 871158. Also, support by grant no. 17-05840S provided by the Grant Agency of the Czech Republic and the project RVO:67985815 is acknowledged. This work used data from the All Sky Automated Survey (ASAS) database, the Catalina Transient Survey, the AAVSO International database (USA), and the AFOEV database (France). I thank the variable star observers worldwide. This research has also made use of observations from the DASCH project at Harvard, partially supported from NSF grants AST-0407380, AST-0909073, and AST-1313370. I also thank Prof. Petr Harmanec for providing me with the HEC13 code. The Fortran source version, compiled version, and brief instructions on how to use the program can be obtained at (http://astro.troja.mff.cuni.cz/ftp/hec/HEC13/).

References

Bailer-Jones, C. A. L., Rybizki, J., Fouesneau, M., Mantelet, G., & Andrae, R. 2018, AJ, 156, 58

Bianchini, A. 1990, AJ, 99, 1941

Bisikalo, D. V., & Zhilkin, A. G. 2012, in IAU Symp., 282, From Interacting Binaries to Exoplanets: Essential Modeling Tools, ed. M. T. Richards & I. Hubeny (Cambridge: Cambridge University Press), 509

Blinova, A. A., Romanova, M. M., & Lovelace, R. V. E. 2016, MNRAS, 459, 2354

Blinova, A. A., Romanova, M. M., Ustyugova, G. V., Koldoba, A. V., & Lovelace, R. V. E. 2019, MNRAS, 487, 1754

Brockwell, P. J., & Davis, R. A. 1987, Time Series: Theory and Methods (New York: Springer-Verlag)

Bruch, A., & Grutter, M. 1997, Acta Astron., 47, 307

Buckley, D. A. H., Meintjes, P. J., Potter, S. B., Marsh, T. R., & Gänsicke, B. T. 2017, Nature Astron., 1, 0029

Cropper, M. 1990, Space Sci. Rev., 54, 195

Drake, A. J., et al. 2009, ApJ, 696, 870

Echevarría, J., Smith, R. C., Costero, R., Zharikov, S., & Michel, R. 2008, MNRAS, 387, 1563

Eracleous, M., & Horne, K. 1996, ApJ, 471, 427

Gänsicke, B. T., et al. 2009, MNRAS, 397, 2170

Gaia Collaboration, 2018, A&A, 616, A1

Garnavich, P., & Szkody, P. 1988, PASP, 100, 1522

Geng, J.-J., Zhang, B., & Huang, Y.-F. 2016, ApJ, 831, L10

- Genzel, R., Schödel, R., Ott, T., Eckart, A., Alexander, T., Lacombe, F., Rouan, D., & Aschenbach, B. 2003, Nature, 425, 934
- Goliasch, J., & Nelson, L. 2015, ApJ, 809, 80
- Grindlay, J., Tang, S., Los, E., & Servillat, M. 2012, in IAU Symp., 285, New Horizons in Time-Domain Astronomy, ed. R. E. Griffin et al. (Cambridge: Cambridge University Press), 29
- Grindlay, J. E., & Griffin, R. E. 2012, in IAU Symp., 285, New Horizons in Time-Domain Astronomy, ed. R. E. Griffin et al. (Cambridge: Cambridge University Press), 243
- Hameury, J.-M., Menou, K., Dubus, G., Lasota, J.-P., & Hure, J.-M. 1998, MNRAS, 298, 1048
- Hellier, C., & Beardmore, A. P. 2002, MNRAS, 331, 407
- Hill, C. A., Watson, C. A., Shahbaz, T., Steeghs, D., & Dhillon, V. S. 2014, MNRAS, 444, 192
- Hill, C. A., Watson, C. A., Steeghs, D., Dhillon, V. S., & Shahbaz, T. 2016, MNRAS, 459, 1858
- Kafka, S., Ribeiro, T., Baptista, R., Honeycutt, R. K., & Robertson, J. W. 2008, ApJ, 688, 1302
- Kafka, S., Tappert, C., Ribeiro, T., Honeycutt, R. K., Hoard, D. W., & Saar, S. 2010, ApJ, 721, 1714
- Kalomeni, B., Nelson, L., Rappaport, S., Molnar, M., Quintin, J., & Yakut, K. 2016, ApJ, 833, 83
- Katz, J. I. 2017, ApJ, 835, 150
- Knigge, C., Baraffe, I., & Patterson, J. 2011, ApJS, 194, 28
- Krzeminski, W., & Serkowski, K. 1977, ApJL, 216, L45
- Littlefield, C., Garnavich, P., Kennedy, M., Callanan, P., Shappee, B., & Holoien, T. 2017, ApJ, 845, L7
- Marsh, T. R., et al. 2016, Nature, 537, 374
- Meintjes, P. J. 2002, MNRAS, 336, 265
- Meyer, L., Eckart, A., Schödel, R., Duschl, W. J., Mužić, K., Dovčiak, M., & Karas, V. 2006, A&A, 460, 15
- Norton, A. J., Butters, O. W., Parker, T. L., & Wynn, G. A. 2007, in AIP Conf. Proc., 924, The Multicolored Landscape of Compact Objects and Their Explosive Origins, ed. L. Angelo Antonelli et al. (New York: AIP), 534
- Norton, A. J., Butters, O. W., Parker, T. L., & Wynn, G. A. 2008, ApJ, 672, 524

- Patterson, J., & Price, C. M. 1981, ApJ, 243, L83
- Pavlenko, E. P. 1996, Odessa Astron. Publ., 9, 38
- Pavlenko, E. P., & Shugarov, S. Y. 1998, A&AT, 15, 89
- Peterson, E., Littlefield, C., & Garnavich, P. 2019, AJ, 158, 131
- Podsiadlowski, P., Han, Z., & Rappaport, S. 2003, MNRAS, 340, 1214
- Pojmanski, G. 1997, Acta Astron., 47, 467
- Rappaport, S., Verbunt, F., & Joss, P. C. 1983, ApJ, 275, 713
- Rosino, L., Romano, G., & Marziani, P. 1993, PASP, 105, 51
- Salazar, I. V., LeBleu, A., Schaefer, B. E., Landolt, A. U., & Dvorak, S. 2017, MNRAS, 469, 4116
- Schenker, K., King, A. R., Kolb, U., Wynn, G. A., & Zhang, Z. 2002, MNRAS, 337, 1105
- Schmidt, G. D., Stockman, H. S., & Grandi, S. A. 1986, ApJ, 300, 804
- Šimon, V. 2013, Acta Polytechnica, 53, 595
- Šimon, V. 2014, in Proc. Frontier Research in Astrophysics, ed. F. Giovannelli & L. Sabau-Graziati PoS(FRAPWS2014) (Trieste: SISSA), 011
- Šimon, V. 2018, in Proc. Frontier Research in Astrophysics III, PoS(FRAPWS2018) (Trieste: SISSA), 058
- Šimon, V. 2019, https://www.plate-archive.org/applause/project/ lswst/lswst1/
- Tapia, S. 1977, ApJ, 212, L125
- van Paradijs, J., Kraakman, H., & van Amerongen, S. 1989, A&AS, 79, 205
- Vondrák, J. 1969, Bull. Astron. Inst. Czechosl., 20, 349
- Wargelin, B. J., Saar, S. H., Pojmański, G., Drake, J. J., & Kashyap, V. L. 2017, MNRAS, 464, 3281
- Warner, B. 1995, Cataclysmic Variable Stars (Cambridge: Cambridge University Press)
- Whittaker, E., & Robinson, G. 1946, The Calculus of Observations (London: Blackie & Son Ltd), 303
- Witzel, G., et al. 2012, ApJS, 203, 18
- Wynn, G. A., King, A. R., & Horne, K. 1997, MNRAS, 286, 436
- Yu, Z., et al. 2019, MNRAS, 489, 1023
- Zamanov, R., & Latev, G. 2017, Bulgarian Astron. J., 27, 19